

LETTER TO THE EDITOR

Whitlockite has a characteristic distribution in mammary microcalcifications and it is not associated with breast cancer

Dear Editor,

Microcalcifications (MCs) are common findings in mammography and can be indicative of different degrees of malignancy, thus requiring multiple stereotaxis vacuum-assisted biopsies under mammography to identify and characterize breast cancer [1, 2]. In many cases, however, the presence of MCs is not associated with the presence of a tumor. Therefore, a better understanding of the physical-chemical properties of MCs is needed to assess the relationship between their presence and breast cancer.

It is known that MCs are mostly composed of hydroxyapatite (HAp), a particular form of calcium phosphate, regardless of the clinical characteristics of the surrounding tissue. However, crystal features of HAp are altered in breast cancer [3]. In addition, other forms of calcium have been more recently identified in breast MCs [4], but their role is yet to be understood.

Whitlockite (Whit) is a magnesium (Mg)-substituted form of calcium phosphate [5], whose presence in breast MCs was suggested as a possible marker of benignity [4] or a marker of invasiveness [6, 7]. In this work, we aimed to determine the relationship between the presence of Whit and the histological and crystal features of MCs and investigate its spatial distribution in breast MCs.

To assess Whit presence in breast MCs, we first performed a correlative mapping study in representative biopsies: one from a healthy tissue (benign), one from ductal carcinoma in-situ (DCIS), and one from an invasive ductal carcinoma (IDC) (Supplementary Figure S1). X-ray fluorescence (XRF) and wide-angle X-ray scattering

(WAXS), both using synchrotron radiation, and Raman spectroscopy were applied to the very same MCs on contiguous tissue sections.

XRF confirmed the presence of Mg confined in calcified areas as a minor component of MCs, quantified relative to phosphorous (P) [Mg mass fraction (w_{Mg}) = 0.005–0.01, P/Mg mass ratio of about 17:1, atomic ratio of about 26:1 to 13:1]. Mg was clearly detected in the three analyzed MCs, regardless of their clinical status (Figure 1A–B). Supplementary Figure S2 shows the distribution of P and Mg in the samples. w_{Mg} maps were derived using a theoretical sample matrix of HAp type-B and the measured sample thickness as calculated from X-ray absorption in each pixel. In the regions close to the MC borders, the Mg mass fraction w_{Mg} was higher than elsewhere in the sample.

We thus performed WAXS analysis on the same selected MCs studied by XRF on contiguous slices. The entire experimental dataset of WAXS spectra was classified using a model-free, statistical approach that identified four characteristic WAXS profiles (Figure 1C–D, Supplementary Figure S3). The first three profiles were associated with HAp with different degrees of crystallinity and abundance. The fourth profile, associated with Whit, was found only in healthy tissue (benign) MCs, mainly located in a rim around the HAp region. By comparing XRF and WAXS data, we observed Mg co-localized with Whit in the healthy tissue (benign), mainly at the boundaries of the MC. On the contrary, Mg detected by XRF in DCIS and in IDC was not associated with Whit.

The Raman mapping analysis of the three selected MCs confirmed the results of the WAXS study. Whit, clearly recognizable by the shift of the phosphate peak at 970 cm^{-1} [4], appeared as a minor component only in the benign sample and distributed around the core of HAp (Figure 1E–F). Raman signals of Whit also localized in the areas where w_{Mg} was higher (XRF) and where the Whit phase was specifically detected by WAXS.

List of abbreviations: MCs, microcalcifications; HAp, hydroxyapatite; Whit, whitlockite; Mg, magnesium; DCIS, ductal carcinoma in-situ; IDC, invasive ductal carcinoma; XRF, X-ray fluorescence; WAXS, Wide Angle X-ray Scattering; P, phosphorous; w_{Mg} , magnesium mass fraction; AUC, area under curve; a- CaCO_3 , amorphous calcium carbonate; c- CaCO_3 , crystalline calcium carbonate (calcite); CaC_2O_4 , calcium oxalate; FWHM, full width at half maximum.

Carlo Morasso and Renzo Vanna authors equally contributed to the work

This is an open access article under the terms of the [Creative Commons Attribution-NonCommercial-NoDerivs](https://creativecommons.org/licenses/by-nc-nd/4.0/) License, which permits use and distribution in any medium, provided the original work is properly cited, the use is non-commercial and no modifications or adaptations are made.

© 2023 The Authors. *Cancer Communications* published by John Wiley & Sons Australia, Ltd. on behalf of Sun Yat-sen University Cancer Center.

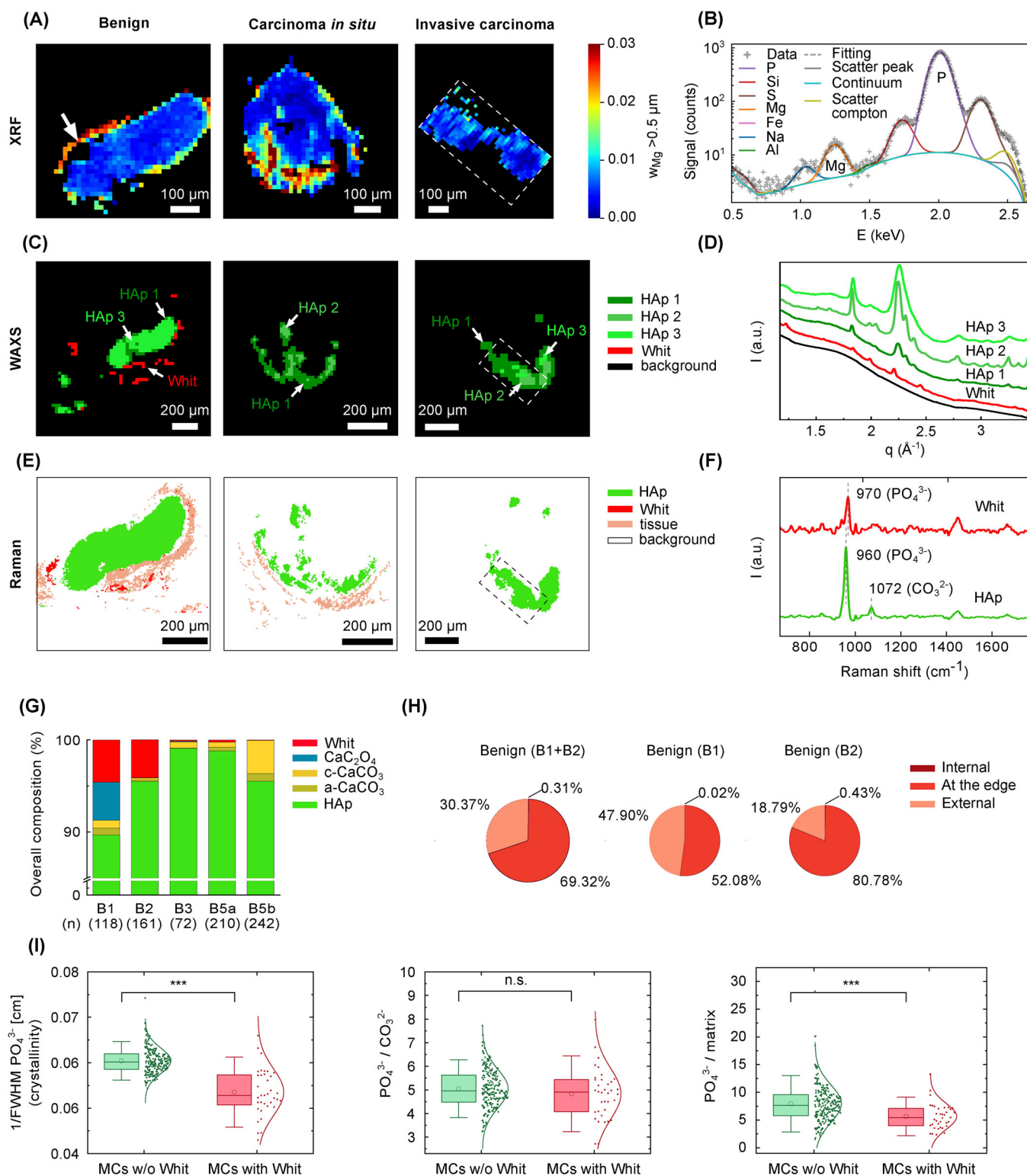


FIGURE 1 Whitlockite is a potential marker of benignity and accumulates mainly around breast MCs. (A) XRF analysis of MCs from representative samples reporting normal tissue (B1), ductal carcinoma in situ (B5a) and invasive ductal carcinoma (B5b), respectively, reporting the Magnesium mass fraction (w_{Mg}) map derived from data taken at 2.5 keV (see Supplementary Figure S2, the intensity maps of P and Mg); values outside the calcifications are plotted as zero; the dashed box defines the same area reported in panels (C) and (E), on contiguous slices. (B) XRF spectra collected at 2.5 keV in the point marked by an arrow in (A). (C) WAXS analysis of contiguous tissue slices reporting the distribution maps of the two crystalline phases: HAp in three shades of green and Whit in red. The different tonalities of green refer to low abundance/high crystallinity HAp (HAp 1, dark green); high abundance/high crystallinity HAp (HAp 2, green); high abundance/low crystallinity HAp (HAp 3, light green). The black area refers to the region of the map where only background signals were

To determine the representative distribution of Whit within breast MCs, we performed a Raman mapping study on 822 MCs from 107 subjects [8]. Of these, 118 MCs were detected in normal tissues or tissues with minimal changes (B1), 169 in samples with benign lesions (B2), 84 in samples with uncertain malignant features (B3), 210 in samples with in-situ carcinoma (B5a), and 241 in samples with invasive carcinoma (B5b). B1 and B2 samples were defined as benign. B3, B5a and B5b samples were defined as malignant. Overall, HAp represented the most abundant mineralized calcium form found in all the datasets (>95%); in B3 and B5a MCs, HAp exceeded 97% of mineralized calcium (Figure 1G, Supplementary Figure S4 and Supplementary Tables S1-S3). In parallel, Whit was detected in 65 MCs and represented the second most abundant mineral in the dataset (2.08% of the overall calcium deposits). Remarkably, Whit was detected almost exclusively in benign samples, where it represented 4.31% of mineralized calcium and was observed in 13 out of 46 benign biopsies (Figure 1G, Supplementary Tables S1-S3). The distribution of Whit was found to be similar in B1 and B2 MCs (B1 = 4.61%; B2 = 4.13%) (Figure 1G, Supplementary Tables S3). On the contrary, only a minimal amount of Whit was detected in malignant samples, where it formed only 0.14% of mineralized calcium. Among malignant samples, Whit was slightly more abundant in B3 (0.12%) and B5a MCs (0.25%) compared to B5b MCs (0.06%) (Figure 1G, Supplementary Tables S3). These rare deposits of Whit were detected in 9 out of the 64 malignant biopsies.

The spatial distribution of Whit detected in all MCs from benign samples is shown in Figure 1H. Most of Whit was located “at the edge” of the HAp core of the MCs (69.32%) in direct contact with HAp, a significant portion

(30.37%) was “external” which presented a physical separation from HAp, and only a minimal portion (0.31%) was “internal” to the HAp core (representative maps in Supplementary Figure S4). This distribution was similar in B1 and B2 samples (Figure 1H), and it confirmed what we observed through the correlative mapping in the three representative samples.

We thus studied the typical Raman spectral characteristics of HAp [4, 9] in benign MCs presenting Whit, compared with those in benign MCs without Whit (Figure 1I). Interestingly, MCs containing Whit showed HAp with lower crystallinity [$p < 0.001$; area under the curve (AUC) = 0.88] if compared with MCs without Whit, and low crystallinity is a marker of benignity [4]. On the contrary, the levels of carbonate inclusions in HAp were comparable in MCs with or without Whit. Lastly, the mineral-to-matrix ratio of the MCs with Whit was significantly lower than that of MCs without Whit in benign tissues ($p < 0.001$; AUC = 0.88) and more similar to that of MCs detected in malignant lesions (Figure 1I, Supplementary Figure S5).

As a limitation, we analyzed the presence of Whit in MCs which were at least 15 μm in size. However, we did not rule out the possibility of smaller Whit deposits elsewhere in the tissues. A recent study reported very small Whit deposits also in invasive breast cancer [10].

In conclusion, our data suggest that the co-presence of Whit and HAp in breast MCs could be a marker of benignity. We also observed that MCs made of HAp in benign tissues are frequently associated with Whit localized at the border of MCs or in the immediate surrounding area. The almost complete absence of Whit in malignant samples may suggest that this specific calcium phosphate phase could be progressively lost with cancer onset. At the same

collected. (D) WAXS signals corresponding to the two crystalline phases and HAp variants mapped in (C). WAXS spectra and pixels in the images are plotted with the same colors (see Supplementary Figure S3, the comparison with theoretical signals). WAXS spectra are shifted for clarity. (E) Raman mapping analysis of tissue slices contiguous to those used for XRF and WAXS studies, reporting in false colors the localization of HAp (green), Whit (red), surrounding tissue (light pink) and background (white). (F) Average Raman spectra of HAp (green) and Whit (red) pixels detected in (E); Raman spectra are shifted for clarity. (G) Mineral composition of the 822 MCs reporting the percentage of each mineral component [Whit (red), calcium oxalate (CaC_2O_4 , blue), crystalline calcium carbonate (i.e. calcite) (c-CaCO_3 , yellow), amorphous calcium carbonate (a-CaCO_3 , beige), and HAp (green)] considering the calcium deposit detected by Raman spectroscopy in the different diagnostic categories [normal tissue or minimal changes (B1); benign (B2); uncertain malignity (B3); in-situ carcinoma (B5a); invasive carcinoma (B5b)] (more details in Supplementary Tables S2-S3). (H) spatial distribution of Whit within benign MCs. Pie charts represent the percentage of Whit pixels detected as “internal”, “at the edge”, or “external” to the HAp core in benign (B1+B2) (left) or in B1 (middle) and B2 MCs (right panel). (I) Statistical analysis of the Raman metrics obtained from the analysis of the HAp core of benign MCs. The three boxplots report the crystallinity (1/full width at half maximum (FWHM) of the phosphate band at 960 cm^{-1}) of HAp in MCs presenting Whit compared to those that do not have Whit (left); the level of carbonate inclusions (measured as the ratio between the phosphate peak at 960 cm^{-1} and the one of carbonate at 1072 cm^{-1}) in HAp in MCs presenting Whit compared to those that do not have Whit (middle); the mineral-to-matrix ratio (measured as the ratio between the phosphate peak at 960 cm^{-1} and the CH_2 peak at 1450 cm^{-1}) in MCs presenting Whit compared to those that do not have Whit (right). Each data point represents a single MC. Empty dot: mean; lines: median; whiskers: 1.5 IQR.

Abbreviations: **MCs**, microcalcifications; **HAp**, hydroxyapatite; **Whit**, whitlockite; **a- CaCO_3** , amorphous calcium carbonate; **c- CaCO_3** , crystalline calcium carbonate (calcite); **CaC_2O_4** , calcium oxalate; **Mg**, magnesium; **P**, phosphorous; **XRF**, X-ray fluorescence; **WAXS**, Wide Angle X-ray Scattering; **FWHM**, full width at half maximum.

time, this process does not necessarily imply the removal of Mg from MCs, as revealed by the XRF detection of Mg in all three diagnostic categories. In future, further studies will be needed to obtain a comprehensive picture of the various calcium deposits in the breast tissues.

DECLARATIONS

AUTHORS' CONTRIBUTION

CM, RV, CG and FC originally conceived the project and wrote the first draft of the paper. FC selected the clinical patients involved. RV, FP and CM collected Raman's data. LF, RV and CM performed the analysis of Raman data. MT and SA performed the statistical analysis. LV and FP prepared the histological sections used in the study. OB and CG analyzed most of the SAXS/WAXS data together, while CG performed the Rietveld analysis. CG, TH, and CB took the XFR data. TH performed the data analysis of the XRF spectra. All authors reviewed the paper.

ACKNOWLEDGMENT

We acknowledge the Paul Scherrer Institut, Villigen, Switzerland for the provision of synchrotron radiation beamtime at the cSAXS and PHOENIX beamlines of the SLS and we gratefully acknowledge the support by Andreas Menzel and further technical support by Xavier Donath. Davide Altamura is acknowledged for sample preparation. The research leading to these results has received funding for the beamtime at the SLS from the European Union's Horizon 2020 research and innovation program under grant agreement No 731019 (EUSMI). This project was supported by the Italian Ministry of Health under the framework of the "Ricerca corrente" project: "Identificazione automatica e non supervisionata di caratteristiche biochimiche specifiche di microcalcificazioni mammarie dai dati di mappatura mediante spettroscopia Raman". We also acknowledge to "Bruno Boerci" biobank for the support in the handling of the clinical samples used in the study.

CONFLICT OF INTEREST STATEMENT

The authors do not have any potential conflict of interest to report.

FUNDING INFORMATION

European Union's Horizon (731019) and Ministero della Salute (Ricerca Corrente).

ETHICS APPROVAL AND CONSENT TO PARTICIPATE

The study was authorized by the Ethical Committee of Istituti Clinici Scientifici Maugeri IRCCS (protocol 2281/2018 CE) and was performed in compliance with the

declaration of Helsinki. All patients provided written informed consent.

CONSENT FOR PUBLICATION

Not applicable.

DATA ACCESS STATEMENT

Data were generated by the authors and available on request.

Carlo Morasso¹ 

Renzo Vanna²

Francesca Piccotti¹

Lidia Frizzi¹


Marta Truffi¹ 

Sara Albasini¹

Camelia Borca³

Thomas Huthwelker³

Laura Villani¹

Oliver Bunk³ 

Cinzia Giannini⁴

Fabio Corsi^{1,5}

¹*Istituti Clinici Scientifici Maugeri IRCCS, Pavia, Italy*

²*National Research Council (IFN-CNR), Institute for Photonics and Nanotechnologies, Milan, Italy*

³*Paul Scherrer Institut, Villigen PSI, Switzerland*

⁴*National Research Council, Institute of Crystallography, Bari, Italy*

⁵*Department of Biomedical and Clinical Sciences, University of Milan, Milan, Italy*

Correspondence

Fabio Corsi, Istituti Clinici Scientifici Maugeri IRCCS, Via Maugeri 4, 27100 Pavia, Italy.
Email: fabio.corsi@icsmaugeri.it

Cinzia Giannini, Institute of Crystallography, National Research Council, Via Giovanni Amendola 122/O, 70126 Bari, Italy.

Email: cinzia.giannini@ic.cnr.it

ORCID

Carlo Morasso  <https://orcid.org/0000-0001-9185-0198>

Marta Truffi  <https://orcid.org/0000-0002-1095-4188>

Oliver Bunk  <https://orcid.org/0000-0001-6563-4053>

REFERENCES

1. Cox RF, Hernandez-Santana A, Ramdass S, McMahon G, Harmey JH, Morgan MP. Microcalcifications in breast cancer: novel insights into the molecular mechanism and functional consequence of mammary mineralisation. *Br J Cancer*. 2012;106(3):525–37.

2. Haka AS, Shafer-Peltier KE, Fitzmaurice M, Crowe J, Dasari RR, Feld MS. Identifying microcalcifications in benign and malignant breast lesions by probing differences in their chemical composition using Raman Spectroscopy. *Cancer Res.* 2002;62(18):5375–80.
3. Gosling S, Scott R, Greenwood C, Bouzy P, Nallala J, Lyburn ID, et al. Calcification microstructure reflects breast tissue microenvironment. *J Mammary Gland Biol Neoplasia.* 2019;24(4):333–42.
4. Vanna R, Morasso C, Marcinnò B, Piccotti F, Torti E, Altamura D, et al. Spectroscopy reveals that biochemical composition of breast Microcalcifications correlates with Histopathologic features. *Cancer Res.* 2020;80(8):1762–72.
5. Dickens B, Schroeder LW, Brown WE. Crystallographic studies of the role of mg as a stabilizing impurity in β -Ca₃(PO₄)₂. the crystal structure of pure β -Ca₃(PO₄)₂. *J. Solid State Chem.* 1974;10(3):232–48.
6. Kunitake JAMR, Choi S, Nguyen KX, Lee MM, He F, Sudilovsky D, et al. Correlative Imaging reveals physiochemical Heterogeneity of Microcalcifications in Human Breast Carcinomas. *J Struct Biol.* 2018;202(1):25–34.
7. Scott R, Stone N, Kendall C, Geraki K, Rogers K. Relationships between pathology and crystal structure in Breast Calcifications: An in Situ X-Ray diffraction study in histological Sections. *Npj Breast Cancer.* 2016;2(1):16029.
8. Caldarone A, Piccotti F, Morasso C, Truffi M, Sottotetti F, Guerra C, et al. Raman analysis of Microcalcifications in male breast cancer. *Spectrochim. Acta. A. Mol Biomol Spectrosc.* 2021;263:120185.
9. Unal M, Ahmed R, Mahadevan-Jansen A, Nyman JS. Compositional assessment of bone by Raman Spectroscopy. *Analyst.* 2021;146(24):7464–90.
10. Kunitake JAMR, Sudilovsky D, Johnson LM, Loh HC, Choi S, Morris PG, et al. Biomineralogical signatures of breast microcalcifications. *Sci Adv.* 2023;9(8):eade3152.

SUPPORTING INFORMATION

Additional supporting information can be found online in the Supporting Information section at the end of this article.